*American Mineralogist, Volume 79, pages 148–153, 1994*

# An experimental simulation of upper mantle metasomatism

NICHOLAS W. A. ODLING
Department of Geology and Geophysics, University of Edinburgh, West Mains Road, Edinburgh EH9 3JW, Scotland

## ABSTRACT

An experimental technique has been devised in which the effects of partial melting and metasomatism are simulated using a piston-cylinder apparatus. Model peridotite (pyrolite minus 40% olivine) and a fluid source were placed in a capsule 12 mm long within a standard piston-cylinder assembly such that the capsule extended downward from the hot spot into the thermal gradient to give a temperature variation of ~100 °C along the capsule. In an experiment conducted at 20 kbar and a maximum temperature of 1175 °C, a variety of phase assemblages was produced. These vary from harzburgite + melt at the high-temperature end to mica + alkali amphibole websterite at the low-temperature end of the capsule. In the upper portion of the capsule the Mg′ [Mg/(Mg + $Fe_{tot}$)] of all the phases decreases as the temperature decreases, and both pyroxene species increase in Al and Ti and decrease in Cr. Near the base of the capsule the trends in Al, Ti, and Mg′ are reversed, and in the lowermost section of the charge abundant alkali amphibole (katophorite) is present with lesser amounts of phlogopite. As far as the author is aware this is the first report of the development of alkali amphibole in unmodified pyrolite. The assemblages bear similarities to those described in metasomatic xenoliths of upper mantle origin.

## INTRODUCTION

The concept of metasomatism as a mechanism of chemical change in the upper mantle continues to be the topic of much discussion (see Harte and Hawkesworth, 1989, for review). In particular, there is still much debate as to both the physical and chemical nature of the metasomatic agent: some workers have envisaged metasomatism as being the result of the movement and interaction of silicate melts with peridotite (e.g., Harte et al., 1977); others, by contrast, have favored models in which the metasomatic agents are fluids dominated by C-O-H components (e.g., Erlank and Shimizu, 1977; Bailey, 1982). The assessment of these two differing concepts has been hampered by a lack of experimental data on the composition of low-degree partial melts on the one hand and the solubility of oxide components in volatile-dominated fluids under mantle conditions on the other. Even if such data were readily available, uncertainty would still remain as to what would be the products of reaction between such fluids and peridotitic assemblages. An alternative approach is to simulate the conditions of metasomatism experimentally by introducing environmental gradients (e.g., thermal or compositional) similar to those envisaged as being the cause of metasomatism. The experiment described here was devised to examine the fractionation and interaction effects induced by a thermal gradient. The objective was to simulate the compositional features that might develop in relatively cool peridotite immediately adjacent to a sheet of injected magma.

## RATIONALE AND EXPERIMENTAL DETAILS

In most piston-cylinder experiments, the need for temperature homogeneity across the sample constrains the size of the capsule to be smaller than the size of the thermal plateau of the experimental assembly used (generally ~5 mm maximum). However, the thermal gradient inherent in the assembly can be used to simulate the thermal gradients that develop in relatively cool country rock adjacent to a body of hot magma.

To simulate the metasomatic effects of such an event in lithospheric mantle, a capsule 12 mm long was constructed (Fig. 1) and placed within a standard assembly for which the thermal profile has been determined. If melting is induced at the high-temperature end of the capsule, then the melt fraction decreases downward from the hot spot. In this situation the components are free to migrate in response to any chemical-potential gradients set up as a consequence of the thermal gradient. Any migration of components is evident from variations in the mineral assemblages developed and in the compositions of the phases. In this second characteristic, comparison must be made with phase compositions obtained from isothermal experiments. For this reason, Hawaiian pyrolite minus 40% olivine component (Green, 1973) was chosen for the bulk composition to allow comparison with the results of an ongoing study of the phase relations of this composition. As hydrous minerals are a prominent characteristic of metasomatic mantle, a C-O-H fluid source was included in the experiment to allow the development of hydrous phases.

0003–004X/94/0102–0148$02.00

**Table 1.** Mg′ of minerals in the assemblages formed in F1–F12

| | Ol | Opx | Cpx | Spl | Grt | Ilm | Rt | Phl | Amph |
|---|---|---|---|---|---|---|---|---|---|
| F1 | 0.8976 | 0.9083 | — | 0.6712 | — | — | — | — | — |
| F2 | 0.8781 | — | — | 0.6843 | — | — | — | — | — |
| F3 | 0.8728 | — | — | 0.6838 | — | — | — | — | — |
| F4 | 0.8718 | 0.8806 | 0.8765 | 0.7312 | 0.7718 | — | 0.5555 | — | — |
| F5 | 0.8523 | 0.8646 | 0.8704 | — | 0.7487 | 0.4765 | 0.6120 | — | — |
| F6 | 0.8583 | 0.8645 | 0.8702 | — | 0.7504 | 0.5569 | 0.6716 | — | — |
| F7 | — | — | 0.8738 | — | 0.7529 | 0.4704 | — | — | — |
| F8 | — | 0.8698 | — | — | 0.7573 | 0.4552 | — | — | — |
| F9 | — | 0.8650 | — | — | — | 0.4372 | — | — | — |
| F10 | — | 0.9087 | 0.8637 | — | — | 0.4162 | — | — | — |
| F11 | — | 0.8821 | 0.8758 | — | — | 0.3951 | — | — | — |
| F12 | — | 0.8780 | — | — | — | 0.2466 | 0.3185 | 0.8919 | 0.8819 |

Two hundred milligrams of the pyrolite were loaded into a graphite capsule and placed in an outer Pt capsule, along with 120 mg of a WC + $WO_2$ + C buffer mixture and 10 mg of a stearate fluid. This arrangement is similar to that developed by Taylor and Foley (1989) for buffering experimental assemblages. In this case, however, only a relatively small amount of buffer assemblage could be used without causing excessive separation of the peridotite from the thermocouple. Thus the assemblage was intended to act as an $f_{O_2}$ monitor only. The capsule was then placed in a heater assembly made with talc, BN, and graphite and the experiment conducted in a piston-cylinder apparatus with a ½-in. bore at the University of Edinburgh. The thermocouple ($Pt/Pt_{87}Rh_{13}$) entered the furnace assembly through a mullite sleeve and was isolated from the sample by a sintered alumina disk 0.5 mm thick. No pressure correction has been applied to the emf of the thermocouple at experimental conditions. A hot piston-in technique with a pressure correction of minus 10% was used to achieve the experimental conditions. After 24 h, the experiment was quenched. The capsule was cleaned, pierced, and placed in an oven for 2 h to allow any volatile components to escape. A weight loss of 7 mg indicates that the experimental assemblage contained ~3 wt% free vapor if one assumes no significant precipitation of hydrous phases from the fluid during quenching. X-ray diffraction analysis of the buffer assemblage showed that none of the phases was exhausted during the experiment; thus, although the mass ratio of mix to buffer was too small to allow efficient buffering, it is probable that the $f_{O_2}$ of the experiment did not deviate significantly from the buffer reaction (log $f_{O_2} \approx$ IW + 1: Taylor and Foley, 1989).

Twelve fragments from the experiment were mounted in epoxy resin with their relative positions preserved, and then sectioned longitudinally (Fig. 1). The fragment number (hereafter referred to as F1, F2, etc.), as shown in Figure 1, gives an indication of the relative temperature, but because the fragments are different sizes, the temperature cannot be assumed to vary linearly with the fragment number.

The compositions of the constituent phases of the sample were determined using a Cameca Camebax electron microprobe operating at an accelerating voltage of 20 kV and a beam current of 5 nA. The count time for each element was 30 s, with a subsequent 15-s background measurement.

## Results

### Textures and mineral assemblages

The sample underwent a temperature range of approximately 100 °C, resulting in a variation in the texture, mineral assemblages, and mineral chemistry with distance from the top of the capsule. Mg′ variation and selected phase compositions are presented in Tables 1 and 2. The sample is everywhere porous (consistent with the presence of a substantial amount of free vapor at high

**Table 2.** Selected mineral analyses

| | Opx | | | Cpx | | Grt | Ilm | | | Amph | Phl |
|---|---|---|---|---|---|---|---|---|---|---|---|
| | F1 | F8 | F12 | F4 | F12 | F8 | F5 | F9 | F11 | F12 | F12 |
| $SiO_2$ | 55.47 | 51.78 | 56.41 | 50.39 | 50.29 | 41.62 | 1.11 | 1.42 | 0.44 | 52.66 | 44.39 |
| $TiO_2$ | 0.22 | 0.90 | 0.24 | 1.38 | 0.77 | 0.73 | 55.91 | 54.99 | 55.26 | 0.90 | 0.16 |
| $Al_2O_3$ | 2.47 | 5.71 | 0.58 | 5.39 | 4.37 | 21.88 | 0.88 | 0.62 | 0.19 | 4.30 | 12.57 |
| $Cr_2O_3$ | 1.07 | 0.79 | 0.18 | 1.03 | 0.77 | 1.55 | 1.17 | 1.26 | 0.77 | 0.70 | 0.90 |
| FeO | 5.99 | 7.46 | 6.04 | 4.01 | 8.66 | 10.01 | 26.45 | 28.41 | 30.47 | 4.63 | 4.83 |
| MgO | 33.37 | 28.70 | 32.89 | 16.02 | 27.53 | 17.52 | 13.51 | 12.22 | 11.17 | 21.43 | 26.47 |
| MnO | 0.09 | 0.09 | 0.04 | 0.12 | 0.06 | 0.27 | 0.15 | 0.16 | 0.28 | 0.08 | 0.26 |
| CaO | 0.86 | 3.57 | 1.26 | 19.53 | 6.21 | 6.70 | 0.27 | 0.66 | 0.20 | 6.00 | 0.00 |
| $Na_2O$ | 0.05 | 0.64 | 0.16 | 0.88 | 1.60 | 0.01 | 0.00 | 0.06 | 0.00 | 5.88 | 2.02 |
| $K_2O$ | 0.03 | 0.15 | 0.15 | 0.03 | 0.33 | 0.02 | 0.03 | 0.00 | 0.00 | 1.28 | 5.93 |
| NiO | 0.09 | 0.13 | 0.14 | 0.08 | 0.18 | 0.05 | 0.37 | 0.38 | 0.28 | 0.10 | 0.25 |
| Total | 99.73 | 99.91 | 98.07 | 98.87 | 100.75 | 100.35 | 99.86 | 100.17 | 99.07 | 97.94 | 98.22 |

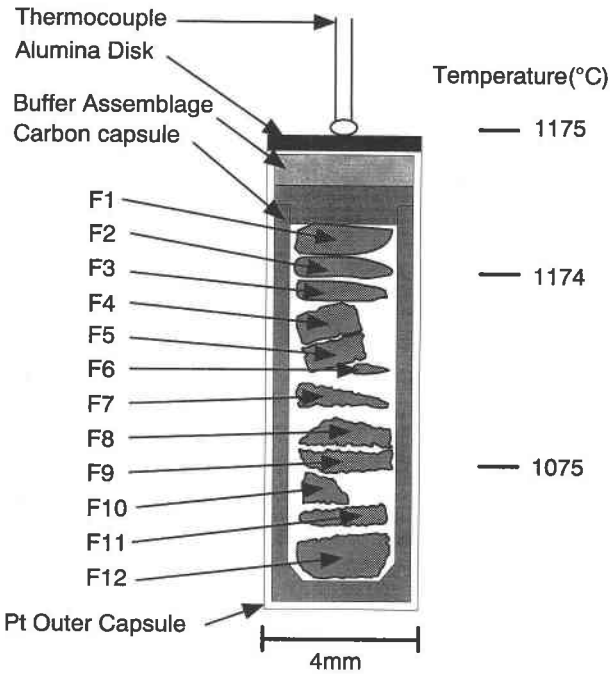


Fig. 1. Partly schematic representation of the capsule design used in the experiment. Outlines show size and location of fragments referred to in text. Numbers to the right indicate temperature.

pressure and temperature), and glass and quench crystals are easily recognizable in fragments from the high-temperature end of the capsule. The amount of quenched melt phases decreases markedly down the sample and cannot be recognized in fragments F5–F12.

**F1-F3: Olivine + orthopyroxene + spinel.** F1 lies within the hot-spot position (1175 °C) and consists of large subhedral to euhedral crystals of olivine, Cr-rich, Al-poor orthopyroxene, and Cr-rich spinel, all of high Mg′ (Table 1) with interstitial glass and quench crystals. With increasing distance from the hot spot, the size of the equilibrium crystals decreases, and there is a drop in the Mg′ of all phases. The spinel becomes increasingly aluminous at the expense of the chromite component.

**F4-F6: Olivine + orthopyroxene ± spinel ± clinopyroxene ± ilmenite ± garnet ± rutile.** Within the F4 fragment aluminous clinopyroxene, pyrope-rich garnet, magnesian ilmenite, and chromian rutile join the assemblage present in F3. Garnet occurs as large equant oikocrysts up to 50 μm in diameter containing inclusions of chromian rutile. Spinel occurs as small euhedral crystals and is less abundant than in F1–F3. In fragment F5 ilmenite appears and spinel is eliminated. The resulting assemblage continues (with a decrease in Mg′) to F6.

**F7-F9: Orthopyroxene + clinopyroxene + garnet + ilmenite.** Olivine is not present in these or any fragments lower in the sample. Garnet and ilmenite (Table 2: analyses 6 and 8, respectively) are locally abundant with lesser amounts of clinopyroxene and orthopyroxene (Table 2: analysis 2), which have greater amounts of Al and Ti and lower amounts of Cr than in F1–F6.

**F10, F11: Orthopyroxene + clinopyroxene + ilmenite.** Orthopyroxene dominates the mineral assemblage of these fragments with lesser amounts of ilmenite and clinopyroxene. Both clinopyroxene and orthopyroxene crystals attain large sizes (up to 20 μm) and contrast with the orthopyroxene of F9 in being markedly poorer in Al, Ti, and Cr. Close examination of backscattered electron images of the clinopyroxene crystals shows them to consist of a fine intergrowth of two phases, on the order of ~1 μm. As the analyses show lower CaO contents than clinopyroxenes from higher temperature regions of the sample but still give acceptable cation totals (4.000 ± 0.015), it is likely that the intergrown phase is orthopyroxene. Ilmenite persists and decreases in Mg′.

**F12: Orthopyroxene + clinopyroxene + mica + amphibole + ilmenite.** Fragment F12 consists of the lowermost portion of the sample and is estimated to have equilibrated at ~1075 °C. The mineral assemblages are dominated by amphibole and mica (Table 2: analyses 10 and 11, respectively) with lesser amounts of orthopyroxene, ilmenite, and rutile. The amphibole is present as characteristic acicular crystals of high Mg′ (0.892) katophorite (nomenclature after Leake, 1978). The mica (Mg′ 0.882) is Na-rich phlogopite that occurs as poikilitic crystals up to 10 μm.

## Interpretation of the modal and chemical variation in the charge

The compositional variations described in the preceding section may be interpreted in at least two ways: (1) the observed variations are all the result of melt-related processes, or (2) the trends present in the lower portion of the charge are a consequence of subsolidus reequilibration and are, therefore, related to interactions between the volatile-rich fluid and the solid phases. While considering the significance of the compositional variations in these alternatives it is essential to bear in mind that the bulk composition of the charge is Hawaiian pyrolite minus 40 wt% olivine. The practice of modifying the modal amount of olivine in peridotite compositions facilitates the analysis of peridotitic assemblages by increasing the amounts of minor phases. This modification is considered to have little effect on the phase compositions, provided olivine saturation is maintained (Falloon and Green, 1988).

Normally the presence of melt in an experimental charge is inferred by a combination of (1) the observation of a quench glass phase, (2) the elimination of a phase from a subsolidus assemblage, or (3) by the marked change in the composition of the phases with changing temperature. These features are, however, approximate at best, as under near-solidus conditions small amounts of melt are difficult to recognize and cause only subtle changes in the composition of abundant phases. Furthermore, elimination of a phase marks the end of a particular melting

reaction, and so the solidus will always lie at some lower temperature. Textural evidence is little better in allowing the recognition of the presence of a melt phase, as the quench products of the vapor-saturated melt (crystals + glass + vesicles) closely resemble the product of subsolidus, vapor-saturated crystallization (crystals + voids ± vapor quench).

It is clear, therefore, that compositional characteristics must be used to establish whether subsolidus conditions prevailed in the lower section of the sample. The position of the solidus may be inferred from the variations of Mg′ (Table 1) and $Al_2O_3$-$Cr_2O_3$ content in orthopyroxene (Fig. 2) with position in the sample. The Mg′ of the orthopyroxene drops steadily from 0.905 at F1 to reach a nearly constant value of 0.865 between F5 and F9. Toward the cooler end of the sample, however, the Mg′ rises steeply, reaching 0.905 in F12. The Mg′ of subsolidus orthopyroxene from isothermal experiments is 0.886 (Odling, unpublished data), and so the rise above this value is inconsistent with partial melting in the charge below F9. The position marking the increase in Mg′ is also marked by a change in the $Al_2O_3$-$Cr_2O_3$ content of orthopyroxene. In the upper portion of the charge (fragments F1–F8) the $Al_2O_3$ content of the orthopyroxene rises systematically while $Cr_2O_3$ drops. Between F8 and F9, however, there is an abrupt change in the alumina content, with only a small decrease in the $Cr_2O_3$, and in fragments F9–F12 the alumina content of the orthopyroxene decreases to values lower than those of F1. On the basis of these compositional variations the orthopyroxenes may be split into two groups, one a high-temperature, high-Al group containing high Cr and Ti and the other a lower temperature, low-Al group containing lower abundances of these elements. It is suggested that the boundary between these two contrasting styles of variation marks the position of the solidus and that the compositional changes present in lower regions of the charge in F9–F12 are the result of fluid-solid reaction. The Al-poor nature of the pyroxenes in F12 may be due to the formation of Al-rich phlogopite; however, because phlogopite is confined to F12, that cannot be the reason for the Al-depleted nature of the pyroxenes from F9–F11 (Fig. 2). It is suggested, therefore, that there has been significant transport of Al via the fluid phase.

Holloway (1971), Schneider and Eggler (1986), and Ryabchikov et al. (1982) have shown that an $H_2O$-rich fluid phase can carry substantial amounts of Si, Al, and alkalis and so is a potentially efficient metasomatic agent. Although the character of the enrichment and depletion effects described here is consistent with the migration of alkalis and Al via the fluid phase, it is probable that the presence of suitable source and sink regions are equally important in the development of the compositional effects. The stable assemblage in the same bulk composition under volatile-present conditions is olivine + Al-rich pyroxenes + pyrope garnet + pargasitic amphibole. Thus, by comparison with the assemblage of two Al-poor pyroxenes + phlogopite + katophorite present in the base

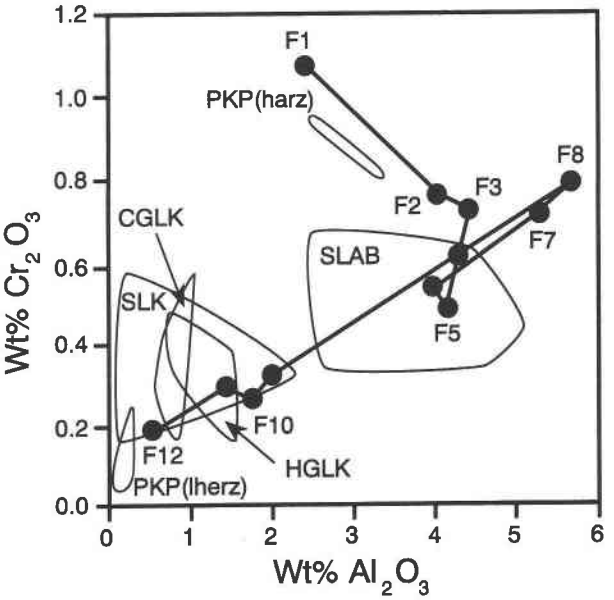


Fig. 2. $Al_2O_3$-$Cr_2O_3$ contents in orthopyroxenes from the experimental sample. Arrows show the progression of compositions from fragment no. 1 (F1) to fragment no. 12 (F12). Marked fields are the compositions of orthopyroxene for xenolith groups taken from Hervig et al. (1986) and Jones et al. (1982) as follows: SLK = spinel lherzolite in kimberlites; SLAB = spinel lherzolite in alkali basalts; HGLK = "hot" garnet lherzolite in kimberlites; CGLK = "cold" garnet lherzolite in kimberlites; PKP(lherz) = phlogopite potassium richterite–bearing lherzolite; PKP(harz) = phlogopite potassium richterite–bearing harzburgite.

of the sample, it is evident that the metasomatic reaction is of the form

$$\text{ol} + \text{grt} + \text{Al-rich px} + \text{fluid} = \text{phl} + \text{amph} + \text{Al-poor px}.$$

Without modal information it is not possible to balance this reaction, but it is similar to the reaction proposed by Erlank and Rickard (1977) for the genesis of phlogopite- and richerite-bearing lherzolite nodules from South Africa. Further work to characterize the mode is being carried out.

## A PRELIMINARY COMPARISON WITH XENOLITH PHASE ASSEMBLAGES

Although a full comparison of the compositional characteristics developed in the experimental sample with those of xenolith suites will be presented elsewhere, several features are worth outlining here. First, a K-enriched assemblage containing abundant amphibole and phlogopite has been produced from a peridotite that, although fertile, is not notably potassic ($Na_2O/K_2O > 5$). Second, the amphibole developed in the base of the charge is of Mg′ 0.892, with (Na + K) > Ca and ($Na_2O + K_2O$) ~ 6.85. This contrasts strongly with the pargasitic amphibole [Mg′ 0.892, (Na + K) < Ca and ($Na_2O + K_2O$) ~ 3.57] that is stable in pyrolite under isothermal, subsoli-

dus conditions at similar temperatures (Green, 1973; Odling, unpublished data). Third, the garnet-absent nature of the amphibole + mica assemblage established in the base of the sample is similar to the PKP xenoliths that have been defined by Erlank et al. (1987) as essentially garnet-free lherzolites or harzburgites containing primary phlogopite and potassium richterite. That contrasts with the garnet-bearing assemblage that is stable in Hawaiian pyrolite at 20 kbar under vapor-saturated, subsolidus conditions (Green, 1973).

Compared with the range of PKP richterite compositions, the amphibole in F12 is richer in FeO by 1.2 wt%, in $Al_2O_3$ by 2.5 wt%, in $TiO_2$ by ~0.5 wt%, and in $Na_2O$ by 1.1 wt% and lower in $K_2O$ by 3.4 wt%. Compared with the lowest pressure mica that is stable in the same bulk composition under isothermal conditions (25 kbar: Odling, unpublished data) the phlogopite in F12 is richer in $Na_2O$ and $SiO_2$ and poorer in $Cr_2O_3$ and $Al_2O_3$. By comparison with the range of phlogopite compositions reported in PKP xenoliths the experimental phlogopite is richer in FeO by 0.5 wt%, in $Na_2O$ by 1.2 wt%, and in $Cr_2O_3$ by 0.4 wt% and poorer in $K_2O$ by 4 wt%.

The uppermost (hottest) Cr-rich, Al-poor orthopyroxene compositions are similar to those found in harzburgites from kimberlites (Fig. 2; Hervig et al., 1986; Jones et al., 1982). With decreasing temperature the trend of decreasing Cr and increasing Al contents approaches that seen in spinel lherzolites in alkali basalts, though the Al contents of the sample orthopyroxene reach slightly higher values at a given Cr content. The pyroxenes of the low-Al group fall close to the fields of orthopyroxenes from spinel and garnet lherzolite, and PKP xenoliths that occur in kimberlites [SLK, CGLK, and PKP (lherz) in Fig. 2] and are similar to the orthopyroxene megacrysts described by Hopps et al. (1989). These features contrast strongly with the pargasite + lherzolite assemblage that is stable in Hawaiian pyrolite at 20 kbar under $H_2O$ vapor-saturated, subsolidus conditions (Green, 1973). There are, therefore, strong similarities between the amphibole + mica–bearing assemblage in the base of the sample and the PKP xenolith suite, both in terms of phase assemblage and phase compositions, particularly as the major difference caused by the lack of olivine in the experimental phase assemblage may be accounted for in the olivine-depleted nature of the pyrolite minus 40% olivine bulk composition. It is possible, therefore, that the PKP metasomatism may be the result of the interaction of peridotite and a volatile-rich fluid expelled from the crystallizing mafic melt rather than a silicate melt itself.

## Conclusions

The assemblages developed in the base of the sample are inferred to have resulted from fluid-saturated, melt-absent conditions and contain alkali-enriched amphibole but are devoid of olivine. The absence of olivine is probably due to increasing silica activity resulting from fractionation, whereas the development of the phlogopite and amphibole is inferred to have resulted from alkali enrichment by the fluid phase. As far as the author is aware, this is the first report of the formation of alkali-rich amphibole in a peridotitic assemblage that, although fertile, is not enriched in K. By analogy with the characteristics of this experiment, it is suggested that the richterite-bearing assemblages in mantle xenoliths are the result of metasomatism caused by an alkali-bearing $H_2O$-rich fluid that may have been derived by reaction and fractionation of a mafic parent melt rather than direct crystallization from a magma at depth.

## Acknowledgments

This research is the result of a research project investigating metasomatic processes supported by NERC grant no. G3/7479. J.B. Dawson, P.D. Kinny, and D. Elthon are thanked for their reviews of earlier drafts of the manuscript.

## References cited

Bailey, D.K. (1982) Mantle metasomatism: Continuing chemical change within the earth. Nature, 296, 525–530.

Erlank, A.J., and Rickard, R.S. (1977) Potassic richterite bearing peridotites from kimberlite and the evidence for kimberlite and the evidence they provide for upper mantle metasomatism. In F.R. Boyd and H.O.A. Meyer, Eds., Extended abstracts volume of the second International Kimberlite Conference, Santa Fe, New Mexico, October 3–7, 1977.

Erlank, A.J., and Shimizu, N. (1977) Strontium and strontium isotope distributions in some kimberlite nodules and minerals. In F.R. Boyd and H.O.A. Meyer, Eds., Extended abstracts volume of the second International Kimberlite Conference, Santa Fe, New Mexico, October 3–7, 1977.

Erlank, A.J., Waters, F.G., Hawkesworth, C.J., Haggerty, S.E., Allsopp, H.L., Rickard, R.S., and Menzies, M. (1987) Evidence for mantle metasomatism in peridotite nodules from the Kimberley pipes South Africa. In M. Menzies and C.J. Hawkesworth, Eds., Mantle metasomatism, p. 221–331. Academic, London.

Falloon, T.J., and Green, D.H. (1988) Anhydrous melting of a fertile and depleted peridotite from 2 to 30 kbar and application to basalt petrogenesis. Journal of Petrology, 29, 1257–1282.

Green, D.H. (1973) Experimental melting studies on a model upper mantle composition at high pressure under water-saturated and water-undersaturated conditions. Earth and Planetary Science Letters, 19, 37–53.

Harte, B., and Hawkesworth, C.J. (1989) Mantle domains and mantle xenoliths. In Kimberlites and related rocks. Geological Society of Australia Special Publication, 14, 649–686.

Harte, B., Cox, K.G., and Gurney, J.J. (1977) Clinopyroxene-rich sheets in garnet peridotite: Xenolith specimens from Matsoku kimberlite pipe, Lesotho. In Extended abstracts volume of the second International Kimberlite Conference, Santa Fe, New Mexico, October 3–7, 1977.

Hervig, R.L., Smith, J.V., and Dawson, J.B. (1986) Lherzolite xenoliths in kimberlites and basalts: Petrogenetic and crystallochemical significance of some minor and trace elements in olivine, pyroxenes, garnet and spinel. Transactions of the Royal Society of Edinburgh: Earth Sciences, 77, 181–201.

Holloway, J.R. (1971) Composition of fluid phase solutes in a basalt-$H_2O$-$CO_2$ system. Geological Society of America Bulletin, 82, 233–293.

Hopps, J.J., Gurney, J.J., Harte, B., and Winterburn, P. (1989) Megacrysts and high temperature nodules from Jagersfontein kimberlite pipe. In Proceedings of the fourth International Kimberlite Conference, Perth. Geological Society of Australia Special Publication, 14, 759–770.

Jones, A.P., Smith, J.V., and Dawson, J.B. (1982) Mantle metsomatism in 14 veined peridotites from Bulfontein mine, South Africa. Journal of Geology, 90, 435–453.

Leake, B. (1978) Nomenclature of amphiboles. American Mineralogist, 63, 1023–1052.

Ryabchikov, I.D., Schreyer, W., and Abraham, K. (1982) Compositions of aqueous fluids in equilibrium with pyroxenes and olivines at mantle temperatures and pressures. Contributions to Mineralogy and Petrology, 79, 80–84.

Schneider, M.E., and Eggler, D.H. (1986) Fluids in equilibrium with peridotite minerals: Implications for mantle metasomatism. Geochimica et Cosmochimica Acta, 50, 711–724.

Taylor, W.R., and Foley, S.F. (1989) Improved oxygen buffering techniques for C-O-H fluid-saturated experiments at high pressure. Journal of Geophysical Research, 94, 4146–4158.

Manuscript received July 13, 1992
Manuscript accepted August 26, 1993